Mathematical and Experimental Evaluation of an Incremental Differential Protection Function Embedded in a Real Transmission Line Relay

L. A. Gama, M. L. S. Almeida, T. R. Honorato, V. R. Serpa and K. M. Silva

***Abstract*—This paper evaluates, mathematically and experimentally, a transmission line differential protection function based on incremental currents, which are not influenced by pre-fault conditions, such as charging and loading levels. In the mathematical analysis, the trajectories for each phase, for all types of faults, are demonstrated by analytic deduction of incremental current ratios. For the experimental assessment, the Alternative Transients Program (ATP) was employed to submit a 500 kV 200 km long transmission line into a wide variety of faults. In addition, a 500 kV transmission line of the Brazilian interconnected system was also modeled via ATP, so that different faults scenarios could be applied to it. Also, for this last set of cases, the algorithm was embedded into a real commercially available relay to assess its performance. In order to carry out a broad evaluation of the incremental algorithm performance, sensitivity analyses were made. The results reveal that the incremental function operates for a bigger variety of faults including ones that the conventional function does not operate.**

***Keywords*—Incremental Differential Protection, Transmission Line, Alpha Plane, Experimental Evaluation, Differential Relay.**

I. Introduction

In order to uphold the electrical power system and all its functions, transmission lines must meet their purpose of interconnecting distant regions by transmitting electrical energy from generation centers to different loads. Due to their large extent and adverse climatic operating conditions, lines are highly exposed to faults, so that it is essential to have safe and modern protection schemes, capable of rapidly eliminating and isolating faults. As the use of numerical relays, combined with modern optical communication systems, has driven the application of differential protection (87L) function for long transmission lines [1], many authors have investigated alternatives to improve its performance, regarding operation problems [2]–[5].

Differential protection performance can be compromised when the system operates at a high loading level [3]. According to [4]–[7], the system loading can impair the analysis of the differential loop. Therefore, the systems operating condition can be a limiting factor for the 87L performance.

With that regard, [6] propose the adjustment of pickup current to values greater than the loading current, so that it does not jeopardize the currents calculated by the differential logic. However, in systems with a significant loading level, the adjustment of the pickup current can result in high values, which is damaging for the protection system sensitivity.

Systems with a high loading level can also compromise the protection performance during high-resistance internal faults, because it can result in outfeed conditions [7]. In this situation, the load current magnitude is greater than the fault current level, such that the differential protection identifies currents lagged by 180° at the terminals, despite being an internal fault. Thus, the traditional percentage differential element will not operate for this internal fault situation. To avoid a misoperation, the authors propose decreasing the slope setting so that the protection scheme becomes more sensitive and able to identify internal faults with outfeed. However, reducing the slope is a risky solution, as it can restrict the protection reliability.

Besides the loading condition, differential protection is also influenced by the capacitive effect, which is associated with intrinsic line characteristics and, therefore, is present during its operation, even before a fault occurs. During steady-state, the line charging current value can be predominant over the loading current, influencing the current transformers (CTs) measurements at the protected line terminals. This situation can generate a false differential current that can lead to a misoperation [8].

Overall, the solutions presented to eliminate the influence of pre-fault conditions, i.e., the decrease in the slope and increase in pickup current, are not feasible as it may cause the differential protection misoperation [9], [10]. Furthermore, logics that depend on voltage measurement were also described to reduce the effects of charging current. However, voltage dependency is not interesting, as the use of capacitive voltage transformers (CVTs) becomes necessary, whereas only CTs would be necessary in the original differential logic.

In [11] and [12], the idea of using incremental differential elements is introduced, once it is demonstrated that pre-fault current removal provides phase elements the same sensitivity of the zero and negative elements. The authors argue that the differential logic must be based on incremental currents, which are defined solely by the fault characteristics and,

The authors would like to thank the Coordination for the Improvement of Higher Education Personnel (CAPES) and the University of Brasília (UnB) for the financial support.

Letícia Gama, Tiago Honorato, Vitor Serpa and Kleber Melo are with the Department of Electrical Engineering at University of Brasília, Brasília-DF, Brazil. Maria Leonor Almeida is with the School of Mechanical, Electrical & Computer Engineering at Federal University of Goiás, Goiânia-GO, Brazil. (e-mail: (leticiagama, tiagohonorato, vitorserpa)@lapse.unb.br, klebermelo@unb.br, marialeonor@ufg.br)

Paper submitted to the International Conference on Power Systems Transients (IPST2021) in Belo Horizonte, Brazil June 06-10, 2021.

therefore, are not influenced by the operating condition of the system. Thus, the currents measured by the CTs must be compensated by calculating the incremental currents in order to ensure the correct differential protection operation. Based on the incremental quantities idea, [13] proposed a differential protection based on incremental complex power alpha plane. Despite elucidating the benefits associated with the use of incremental quantities and presenting satisfactory results, the proposed algorithm is based on incremental complex power and, therefore, voltage measurement is also necessary.

Furthermore, [11] and [12] investigate the possible trajectories of phase elements on the alpha plane against the influence of the following parameters: CT saturation for external faults, fault resistance value and system loading condition. In [11], current ratios equations for phase elements, considering a single-phase short circuit in phase A for a short line, are deduced. Despite performing several types of analyses on the behavior of the differential trajectories, the author deduced only the equations of the differential elements for single-phase to ground short-circuits.

This paper extends the study presented in [11] by analyzing the phase current ratios trajectories behavior for conventional and incremental differential protection, considering all four types of faults. This way, it is possible to infer exactly how different operation conditions interfere on conventional and incremental elements. In order to evaluate the incremental differential algorithm, computational analyses were carried out over a 500 kV/60 Hz and 200 km transmission line test system, modeled on Alternative Transients Program (ATP), considering a wide variety of faults. In this first set of simulations, fault scenarios obtained by varying fault resistance, fault location, source-to-line impedance ratio and system loading were considered. Later, a real Brazilian transmission line, 500 kV/60 Hz and 335 km long, was modeled with the ATP software. In the real system, fault scenarios, obtained by varying fault resistance and location, were considered as input signals for a commercially available relay, through which the incremental algorithm was implemented and tested. All the obtained results highlight the efficient performance of the incremental differential elements in relation to all cases of fault and system characteristics variation assessed.

II. Line Differential Protection

Kirchhoff's first law establishes that the algebraic sum of currents entering and leaving a determined region must equal zero. Based on this principle, line differential protection performs the comparison between phase currents measured in both line ends, referred as local, $\hat{I}_{\phi,L}(k)$, and remote currents, $\hat{I}_{\phi,R}(k)$, where ϕ can represent the phases A, B and C. Also, k represents the k-th sample.

The comparison between local and remote currents started to be implemented based on the operational plane. Alternatively to the operational plane, the alpha plane was proposed in order to better represent the relationship between the phasor quantities involved in the differential function [14]. The alpha plane is a complex plane of the ratio between remote and local currents, and it is traditionally implemented with a circular restraint region. The use of the alpha plane has drawn the attention of manufacturers as it has greater flexibility and, if well adjusted, can protect transmission lines against a wide variety of fault conditions.

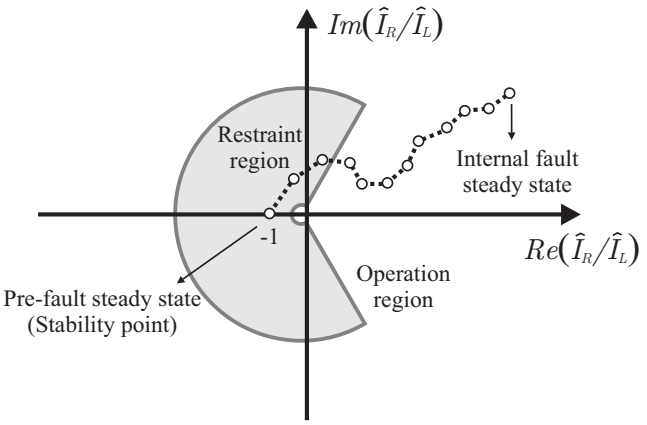

Fig. 1: Differential Element Trajectory on Alpha Plane [2].

Another advantage of the alpha plane is the possibility of determining specific locations of the current ratios for different operating conditions of the system, which does not occur in the operational plane. In this sense, specific regions on the alpha plane can be pre-determined for representing internal and external faults, normal load conditions and also for internal faults with outfeed happening in any terminal. So, an analysis on the settlement regions of the current ratios and their trajectories on the alpha plane, considering the variation of the system parameters, collaborates in the definition of a sensitive, safe and reliable restraint characteristic.

In this context, the modified restraint characteristic, also called modified rainbow characteristic, was proposed [2]. As the modified characteristic is defined by the angle and the radius parameters, it gives greater control over its shape and, consequently, greater reliability.

Traditionally, the alpha plane is based on the ratio of current phasors measured at line terminals. The behavior of these ratios, called Γ, is presented in Fig. 1, where the restraint region is defined as the internal area of the modified rainbow characteristic, whereas the external area corresponds to the operation region. Thus, for any internal fault, Γ moves from the stability point, at $(-1;0)$, to the operation region, allowing fault detection. For external faults, Γ may leave the $(-1;0)$ locus, but it must continue inside the restraint region.

The conventional differential protection, called 87L, is based on the combination of three phase elements: 87LA, 87LB and 87LC. The ratio of these elements is defined by (1) and it is further referred as conventional differential element (CDE). For the sake of simplicity, only the local CDE is shown, since the one attributed to the remote terminal has similar equation.

$$\Gamma_{\phi,L}(k) = \frac{\hat{I}_{\phi,R}(k)}{\hat{I}_{\phi,L}(k)} \tag{1}$$

From the alpha plane analysis in the face of internal and external faults, it is possible to inspect the sensitivity of its

CDEs by investigating their trajectories on the alpha plane for different operating conditions of the system.

III. Line Incremental Differential Protection

Incremental differential protection, called Δ87L is based on the combination of three phase elements: Δ87LA, Δ87LB and Δ87LC. The ratio is portrayed in (2) and it is further referred as incremental differential element (IDE). As it can be seen, the incremental element is basically the subtraction of $\hat{I}_{\phi_{pre}}$, the pre-fault current, from the total fault current, $\hat{I}_{\phi}(k)$, at the instant k. Consequently, the IDEs do not carry the pre-fault information and so, they are inherently incremental. For the sake of simplicity, only the local IDE is shown, since the one attributed to the remote terminal has similar equation.

$$\Gamma_{\Delta\phi,L}(k) = \frac{\hat{I}_{\phi,R}(k) - \hat{I}_{\phi,R_{pre}}}{\hat{I}_{\phi,L}(k) - \hat{I}_{\phi,L_{pre}}} \tag{2}$$

A. Current Contributions Equations

As described in (1) and (2), the ratio computation, both in function 87L and Δ87L, depends on the current contributions coming from each terminal of the transmission line. As the CDEs and IDEs behavior defines their trajectory in the alpha plane, the current contributions of the local and remote terminals, $\hat{I}_{\phi,L}(k)$ and $\hat{I}_{\phi,R}(k)$ respectively, are evaluated. Moreover, according to [11], factors such as line loading, source-to-line impedance ratio and fault resistance employ deviations on the CDEs trajectories. In this context, it is evaluated how these factors influence the current contributions from both line ends and therefore in the trajectories of both differential elements.

Fig. 2 depicts a short transmission line with impedance, Z_L, and local and remote Thévenin impedance equivalents Z_{S_L} and Z_{S_R}. After fault occurrence, the currents entering the line from both sources consist of two parts: load current and pure fault contribution. As states the superposition theorem, these components can be calculated separately solving the system from Fig. 3 before and during the fault. It is emphasized that only the positive sequence circuit is presented and, except for the sources, the remaining circuits are identical to it.

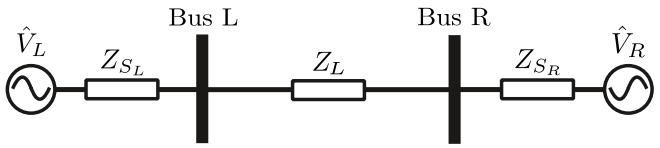

Fig. 2: Short Transmission Line System

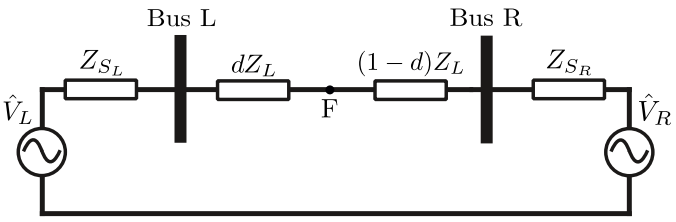

Fig. 3: Positive-Sequence Circuit

For pre-fault steady state, load current $\hat{I}_{LD}$ can be calculated using (3), with $\hat{V}_L$ and $\hat{V}_R$ being the pre-fault local and remote source voltages, and the subscript $j = 1$. To determine the fault currents, the Thévenin equivalents of the sequence networks are needed and these are obtained according to (4) and (5). The parameter *d* in Fig. 3 represents the percentage of the line at which faults are applied, starting from the local terminal.

$$\hat{I}_{LD} = \frac{\hat{V}_L - \hat{V}_R}{Z_{jM} + Z_{jN}} \tag{3}$$

where:

$$Z_{jM} = Z_{S_L} + d \cdot Z_L \tag{4}$$

$$Z_{jN} = Z_{S_R} + (1-d) \cdot Z_L \tag{5}$$

For fault condition solutions, it is necessary to determine the pre-fault voltage at fault point, $\hat{V}_F$, and the fault equivalent impedance Z_j. The former can be obtained through (6), and the latter considering (7), where j can be 0, 1 and 2, for zero, positive and negative sequences, respectively.

$$\hat{V}_F = \hat{V}_L - Z_{1M} \cdot \hat{I}_{LD} \tag{6}$$

$$Z_j = \frac{Z_{jM} \cdot Z_{jN}}{Z_{jM} + Z_{jN}} \tag{7}$$

Based on the type of fault, the sequence networks are connected to obtain the fault currents $\hat{I}_{Fj}$ at the fault location. The current distribution factors, displayed in (8), are used to calculate the sources contributions to the fault. Also, $\hat{I}_{LD}$ is added to positive sequence current, so that local and remote sequence total fault currents, shown in (9) and (10), can be obtained. Finally the sequence fault currents are transformed into phase quantities through the Fortescue matrix, dependent on operator a which is equal to $1\angle 120°$, resulting in the total currents seen by local and remote relays, $\hat{I}_{L,\phi}$ and $\hat{I}_{R,\phi}$.

The phase fault currents contributions for each terminal and fault type are presented in Table I, where "D" is established as (11), which considers the fault resistance influence by means of the phase-to-phase fault resistance (R_P) and phase-to-ground fault resistance (R_G).

$$C_j = \frac{Z_{jN}}{Z_{jM} + Z_{jN}} \tag{8}$$

$$\hat{I}_{L,j} = C_j \cdot \hat{I}_{Fj} \tag{9}$$

$$\hat{I}_{R,j} = (1 - C_j) \cdot \hat{I}_{Fj} \tag{10}$$

$$D = \frac{(Z_0 + R_P + 3R_G)}{Z_0 + Z_2 + 3R_G + 2R_P} \tag{11}$$

B. Alpha Plane Ratios - Elements Trajectories

In order to evaluate the trajectories on the alpha plane, the ratios of local and remote currents must be calculated. This step is done for every phase element of 87L and Δ87L functions, resulting in six differential elements. Table II

TABLE I: Relay Currents.

AG Fault Local Currents	AG Fault Remote Currents
$\hat{I}_{L,A} = (C_0 + C_1 + C_2) \cdot \hat{I}_{F1} + \hat{I}_{LD}$	$\hat{I}_{R,A} = (3 - C_0 - C_1 - C_2) \cdot \hat{I}_{F1} - \hat{I}_{LD}$
$\hat{I}_{L,B} = (C_0 + a^2 C_1 + aC_2) \cdot \hat{I}_{F1} + a^2 \hat{I}_{LD}$	$\hat{I}_{R,B} = \left[1 - C_0 + a^2(1 - C_1) + a(1 - C_2)\right] \cdot \hat{I}_{F1} - a^2 \hat{I}_{LD}$
$\hat{I}_{L,C} = (C_0 + aC_1 + a^2 C_2) \cdot \hat{I}_{F1} + a\hat{I}_{LD}$	$\hat{I}_{R,C} = \left[1 - C_0 + a(1 - C_1) + a^2(1 - C_2)\right] \cdot \hat{I}_{F1} - a\hat{I}_{LD}$
BC Fault Local Currents	**BC Fault Remote Currents**
$\hat{I}_{L,A} = (C_1 - C_2) \cdot \hat{I}_{F1} + \hat{I}_{LD}$	$\hat{I}_{R,A} = (C_2 - C_1) \cdot \hat{I}_{F1} - \hat{I}_{LD}$
$\hat{I}_{L,B} = (a^2 C_1 - aC_2) \cdot \hat{I}_{F1} + a^2 \hat{I}_{LD}$	$\hat{I}_{R,B} = \left[a^2(1 - C_1) - a(1 - C_2)\right] \cdot \hat{I}_{F1} - a^2 \hat{I}_{LD}$
$\hat{I}_{L,C} = (aC_1 - a^2 C_2) \cdot \hat{I}_{F1} + a\hat{I}_{LD}$	$\hat{I}_{R,C} = \left[a(1 - C_1) - a^2(1 - C_2)\right] \cdot \hat{I}_{F1} - a\hat{I}_{LD}$
BCG Fault Local Currents	**BCG Fault Remote Currents**
$\hat{I}_{L,A} = [-C_0(1 - D) + C_1 - C_2 D] \cdot \hat{I}_{F1} + \hat{I}_{LD}$	$\hat{I}_{R,A} = [-(1 - C_0)(1 - D) + (1 - C_1) - (1 - C_2)D] \cdot \hat{I}_{F1} - \hat{I}_{LD}$
$\hat{I}_{L,B} = \left[-C_0(1 - D) + a^2 C_1 - aC_2 D\right] \cdot \hat{I}_{F1} + a^2 \hat{I}_{LD}$	$\hat{I}_{R,B} = \left[-(1 - C_0)(1 - D) + a^2(1 - C_1) - a(1 - C_2)D\right] \cdot \hat{I}_{F1} - a^2 \hat{I}_{LD}$
$\hat{I}_{L,C} = \left[-C_0(1 - D) + aC_1 - a^2 C_2 D\right] \cdot \hat{I}_{F1} + a\hat{I}_{LD}$	$\hat{I}_{R,C} = \left[-(1 - C_0)(1 - D) + a(1 - C_1) - a^2(1 - C_2)D\right] \cdot \hat{I}_{F1} - a\hat{I}_{LD}$
ABC Fault Local Currents	**ABC Fault Remote Currents**
$\hat{I}_{L,A} = C_1 \cdot \hat{I}_{F1} + \hat{I}_{LD}$	$\hat{I}_{R,A} = (1 - C_1) \cdot \hat{I}_{F1} - \hat{I}_{LD}$
$\hat{I}_{L,B} = a^2 C_1 \cdot \hat{I}_{F1} + a^2 I_{LD}$	$\hat{I}_{R,B} = a^2(1 - C_1) \cdot \hat{I}_{F1} - a^2 \hat{I}_{LD}$
$\hat{I}_{L,C} = aC_1 \cdot \hat{I}_{F1} + a\hat{I}_{LD}$	$\hat{I}_{R,C} = a(1 - C_1) \cdot \hat{I}_{F1} - a\hat{I}_{LD}$

contains the equations of the CDEs and IDEs ratios for each fault type: AG fault, BC fault, BCG fault, and ABC fault.

It can be seen that the coefficients of healthy phases stay at the stability point $(-1; 0)$ as the ratios showcase a steady -1 result, independently of the differential function employed. For the affected phases, it is shown that CDE ratios depend on current distribution coefficients, load current, fault current and the term "D", which in turn subjects to the R_P and R_G.

For the incremental element, regarding the AG, BC and ABC faults the IDEs of the faulted phases depend only on current distribution coefficients. For BCG faults, besides the C_j, the IDE depends on "D". In such way, Δ87L elements mostly do not depend on the value of the fault resistance or the system load, as it is the case with CDEs.

Note that the only difference between CDE and IDE ratios is that the second one does not have the $\hat{I}_{LD}/\hat{I}_{F1}$ term, since the load current is subtracted, according to (2).

IV. Simulations and Experimental Results

All the simulations contemplated the same transmission line modeling characteristics on ATP. The long transmission line was implemented as perfectly transposed and considering Clarke model, with distributed and constant in frequency parameters [15]. Besides, in order to employ the CDEs deductions originated from the short line model, highlighted on Table II, on the long transmission line analysis, a method to compensate the capacitive current was applied so that the obtained behavior is similar to a short line [16].

In order to primarily evaluate the incremental differential algorithm, a simplified 500 kV/60 Hz system with a 200 km single circuit transmission line, connected to Thevénin equivalents at its ends, similar to Fig 2, was assumed and modeled via ATP. The algorithm was implemented using a sampling rate of 16 samples per cycle, and the output signals obtained from electromagnetic transients are filtered by means of a third-order low-pass filter, with a cutoff frequency of 180 Hz. The system was submitted to a wide variety of faults by means of computational sensitivity analyses, and fault scenarios were obtained by varying fault resistance (R_G), fault location (d), source-to-line impedance ratio (SIR) and system loading (δ), resulting in a total of 157 events as described in Table III. It is important to mention that the results are based on the evaluation of CDEs and IDEs alpha plane ratios, considering the steady-state fault quantities (i.e. no transient response is considered).

Later, the real 500 kV/60 Hz and 335 km transmission line, located between Teresina II and Sobral III substations in Brazil, was modeled via ATP [17]. A high system loading condition $\delta = 25^\circ$ was considered and it is worthy to point out that this condition was imposed on the system in favor of a more challenging scenario, considering more diverse conditions were evaluated on prior results. As depicted on Fig. 4, the monitored transmission line is one of the two circuits present on a double circuit transmission line. However, it is important to note that the zero-sequence mutual coupling effect was not considered, such that each circuit could be treated as a single circuit transmission line. Besides, as one can see from Fig. 5, the evaluated transmission line is a part of a ring system, which increases the complexity of the analyzed system as a whole. Apart from the line ends, four other terminals, also displayed on Fig. 5, were modeled and directly connected to their Thevénin equivalent sources. Also, transfer impedances, present due to the ring system configuration, were obtained and considered in order to guarantee an accurate ring system modeling.

The evaluation of fault scenarios from the real system was accomplished through sensitivity analyses of fault resistance and fault location variation, resulting in a total of 575 events. It is noteworthy to point out that the obtained results are related to the relays trip from CDE (embedded to the commercial relay) and from IDE (proposed by the authors and implemented on the commercial relay) during fault conditions.

TABLE II: Conventional and Incremental Differential Elements.

Element	AG Fault	BC Fault	BCG Fault	ABC Fault
87LA	$\frac{3}{(C_0+C_1+C_2)+\frac{\hat{I}_{LD}}{\hat{I}_{F1}}}-1$	-1	-1	$\frac{1}{C_1+\frac{\hat{I}_{LD}}{\hat{I}_{F1}}}-1$
Δ87LA	$\frac{3}{(C_0+C_1+C_2)}-1$	-1	-1	$\frac{1}{C_1}-1$
87LB	-1	$\frac{1-a^2}{C_1-a^2C_2+\frac{\hat{I}_{LD}}{\hat{I}_{F1}}}-1$	$\frac{1-a(1-D)-a^2D}{C_1-a\,C_0(1-D)-a^2C_2D+\frac{\hat{I}_{LD}}{\hat{I}_{F1}}}-1$	$\frac{1}{C_1+\frac{\hat{I}_{LD}}{\hat{I}_{F1}}}-1$
Δ87LB	-1	$\frac{1-a^2}{C_1-a^2C_2}-1$	$\frac{1-a(1-D)-a^2D}{C_1-a\,C_0(1-D)-a^2C_2D}-1$	$\frac{1}{C_1}-1$
87LC	-1	$\frac{1-a}{C_1-a\,C_2+\frac{\hat{I}_{LD}}{\hat{I}_{F1}}}-1$	$\frac{1-a^2(1-D)-a\,D}{C_1-a^2C_0(1-D)-a\,C_2D+\frac{\hat{I}_{LD}}{\hat{I}_{F1}}}-1$	$\frac{1}{C_1+\frac{\hat{I}_{LD}}{\hat{I}_{F1}}}-1$
Δ87LC	-1	$\frac{1-a}{C_1-a\,C_2}-1$	$\frac{1-a^2(1-D)-a\,D}{C_1-a^2C_0(1-D)-a\,C_2D}-1$	$\frac{1}{C_1}-1$

TABLE III: Simulated Fault Scenarios.

Fault Type	d (%)	R_G (Ω)	SIR_L	SIR_R	δ
AG	50	R_G^*	0.1	0.1	5°
ABC	50	0.0	1.0	1.0	δ^*
BCG	d^*	10.0	0.1	0.1	5°
AG	50	0.0	SIR_L^*	0.1	5°

Legend:
d^*, R_G^*, SIR_L^* and δ^* stands for the parameters that are varied and later thoroughly acknowledged in this paper.

In order to do so, a database of fault scenarios was reproduced via traditional playback procedures employing a protective relay test equipment set, which was connected to commercially available relays. To assess the Δ87L performance, the protection algorithm was directly integrated on the relay via its embedded programming interface. This area allows the user to access digital and analog quantities, used by the relays native functions, aiming to create additional logics, extend and customize the protection operation, as well as the possibility to integrate other algorithms. Also, the programming interface uses the same processing interval of the relays native protection elements, and consequently it supports an equal comparison between 87L and Δ87L.

For both evaluated systems modeled by means of ATP, current signals were obtained by means of C800 2000-5 CTs, installed at both line terminals, with modeling characteristics and parameters described by [18]. Moreover, voltage signals were measured via CVTs, also connected at both line ends, and modeled as presented in [19].

A. Computational Analysis

Fig. 6 depicts the alpha plane for CDEs and IDEs considering an AG fault with fault resistance, R_G, varying from 0 to 1000 Ω with steps of 10 Ω. It can be noted from Fig. 6a that the CDE fails to detect the fault for R_G larger than 420 Ω. Analyzing the IDEs on Fig. 6b, the advantages are evident since the phase element involved on the short circuit never loses its sensitivity when varying the fault resistance.

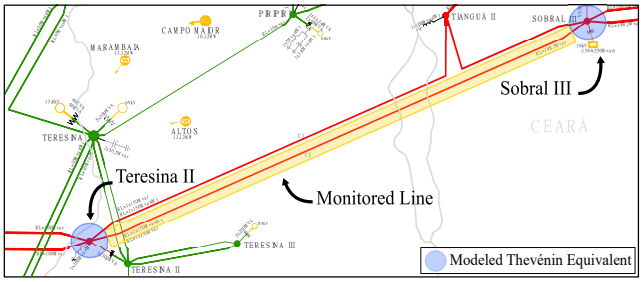

Fig. 4: Monitored Transmission Line System

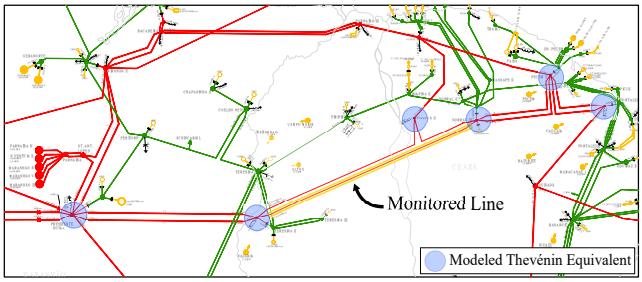

Fig. 5: Monitored Ring System

This behavior favors the use of single-pole tripping schemes since the phase selection is inherent to this category of protection [11]. Also, the healthy phase elements, from both 87L and Δ87L elements, stay correctly put at $(-1;0)$.

The results of an ABC fault with loading conditions, δ, varying from -90° to +90°, in 5% increments, are presented in Fig. 7. It is noteworthy to point out that the CDEs have their performances restricted by a range of -25° to +25° for all phases. Also, the three phase elements have similar behavior, since their trajectories become overlap. From Fig. 7b, it can be concluded that the use of IDEs provides a correct operation for all the load conditions analyzed, making it not influenced by them.

Fig. 8 depicts the alpha plane elements considering a BCG

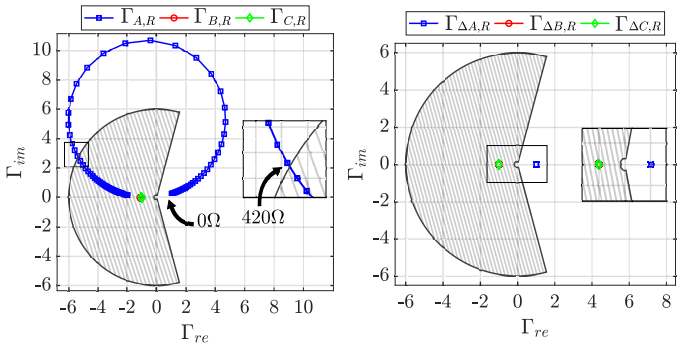

(a) 87L Element (b) Δ87L Element

Fig. 6: Variation of R_G for an internal AG Fault.

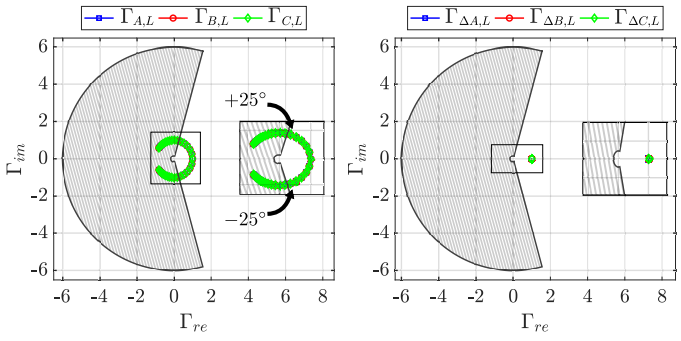

(a) 87L Element (b) Δ87L Element

Fig. 7: Variation of δ for an internal ABC Fault.

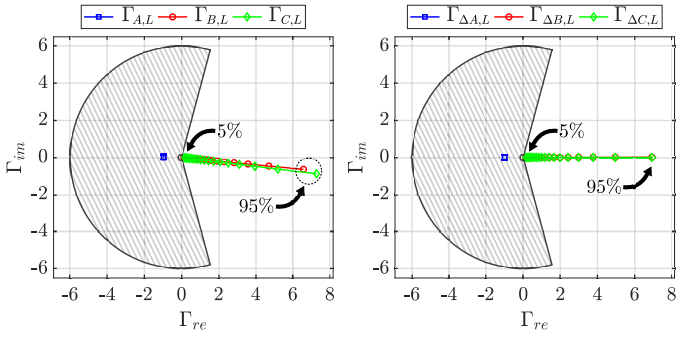

(a) 87L Element (b) Δ87L Element

Fig. 8: Variation of fault location for an internal BCG Fault.

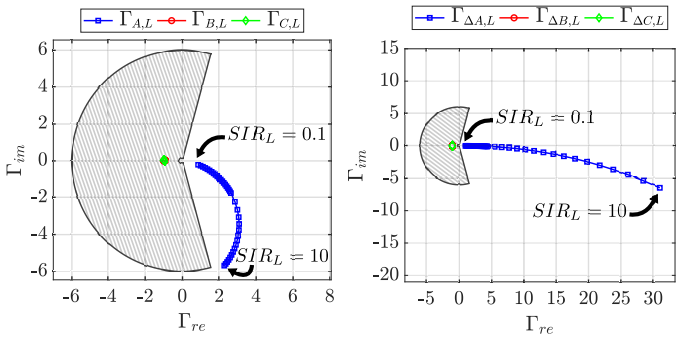

(a) 87L Element (b) Δ87L Element

Fig. 9: Variation of SIR_L for an internal AG Fault.

fault with fault location, d, varying from 5 to 95% with a rate of 5%. It can be seen that as the fault approaches the remote terminal, the greater is the current ratio magnitude on the alpha plane, for both faulted phases CDEs and IDEs. Therefore, the closer the fault is to the local terminal, the lower the value of the differential element magnitude. Furthermore, based on Fig. 8a, it is verified that the imaginary parts of the CDEs ratios are affected by the variation of fault location, which does not happen with IDEs ratios, as seen in Fig. 8b. It is noteworthy that although only the behavior for a BCG fault was presented, the proposed differential protection operated correctly for all simulated fault locations, considering phase-to-ground, phase-to-phase and three-phase faults. Furthermore, the proposed logic is also capable of identifying faulted phases, enabling the implementation of single-phase reclosing scheme.

The results for an AG fault with local source-to-line impedance ratio (SIR_L) varying from 0.1 to 1.0 with steps of 0.1, and from 1.0 to 10 with steps of 1.0, are exhibited in Fig 9. The CDE of phase A is affected, as shown in Fig. 9a, and sustain a rotation course that occurs due to the reduction of the total fault current, as well as the local current contribution. It is noticeable that this rotation tends to make the trajectory carried out by the CDE falls into the restraint characteristic. On the other hand, for the IDE, the rotation observed in Fig. 9a is smoothed, resulting in a trajectory that does not tend to enter on the restraint area. It can also be seen from Fig. 9b that the weaker the local source ($SIR_L \geq 1$) is, the smaller is its contribution to the fault current and, therefore, the greater is the magnitude of IDE ratio related to the faulted phase.

Obtained results can still be analyzed based on the equations presented in Table II. It is verified from the fault resistance variation case, that the CDE ratio trajectory is influenced by the R_G value, as presented in Fig. 6a. This is explained through the $\Gamma_{A,L}$ equation, which depends on $\hat{I}_{F1}$, in turn affected by the R_G value. In opposition, IDE does not change and remains stable in the operating zone, and its behavior is explained through the $\Gamma_{\Delta A,L}$ equation, that does not dependent on term "D", and so it is not influenced by the fault resistance. With the analysis of the system loading variation case, it is demonstrated that the CDEs ratio trajectories change depending on the δ value, as exposed in Fig. 7a. This is clarified via the $\Gamma_{\phi,L}$ equation and its liability on $\hat{I}_{LD}$. On the other hand, IDEs do not change and remain stable in the operating zone. A consistent behavior taking into account the $\Gamma_{\Delta\phi,L}$ equation does not depend on loading conditions.

From the fault location and source-to-line impedance ratio variation cases, it can be seen from Fig. 8 and 9 that both CDE and IDE trajectories are influenced by d and SIR_L values. Based on Table II, it is verified that $\Gamma_{\phi,L}$ and $\Gamma_{\Delta\phi,L}$ for faulted phases depend on C_j, which in turn depends on the values of $Z_{j,M}$ and $Z_{j,N}$, that are influenced by the location and the source-in-line impedance ratio as described in (4) and (5).

B. Experimental Analysis

For the experimental tests on the real transmission line, AG and BC faults were examined for two sets of sensitivity analyses. The results display 87L and Δ87L performance,

which are demonstrated through phase A element trip signal, regarding the AG fault, and by the simultaneously trip signal emission from both phase B and C elements, for the BC fault condition. The first sensitivity analysis test contemplated a fault location variation, considering the range of 1% to 99% and steps of 1%, during an A-to-ground solid fault and also for a BC solid fault. For the second sensitivity analysis test, the fault was applied in the middle of the line and considering fault resistance value range of 0 Ω to 500 Ω and 0 Ω to 250 Ω, with steps of 2 Ω, for an A-to-ground fault and for a BC fault, respectively. The obtained results are evaluated by means of operating time for both protection functions assessed in these cases, as one can see from Fig. 10 to Fig. 13.

It is noticeable from Fig. 10, correspondent to the AG solid fault location variation analysis, that both CDE and IDE correctly operate for all cases, as foreseen in Fig. 8. The highlight from this case is that the incremental element, $\Delta 87L$, presents a more stable and evenness trajectory, as noticed by its distribution profile. While, conventional element trajectory presents a more scattered distribution profile.

As shown in Fig. 11, related to the fault location variation analysis for the BC fault, CDE and IDE correctly operate for all cases, displaying similar behavior to Fig. 10. Also, $\Delta 87L$ element presents a stable trajectory, in conformity with its distribution profile. Contrarily, a more scattered distribution profile is displayed by conventional elements trajectory.

Fig. 12 reveals that the IDE correctly emits a trip signal for every fault resistance evaluated considering the A-to-ground fault. This can be explained by the incremental element equation exhibited in Table II and how it does not depend on the term "D". As for fault resistances over 50 Ω, the CDE was no longer triggered, since this element is also affected by the loading conditions. In order to improve its performance, the relay pickup setting for the phase differential function was adjusted to its minimal value and the fault resistance sensitivity analysis was executed again. The obtained results revealed that the CDE continued to misoperate for values over 50 Ω.

Interpretation of the results presented on Fig. 13, obtained when fault resistance values are varied considering the BC fault, reveals its similarity to the performance shown in Fig. 12. The IDE correctly emits a trip signal for every evaluated case. On the other hand, cases with fault resistances over than 175 Ω did not triggered the CDE, since this element is also influenced by pre-fault conditions.

In addition to the simulations described, for the real system it was also evaluated the CDE and IDE performance during two different bolted external faults with CT saturation: phase-to-ground and three-phase faults. The CT saturation was modeled considering 100 Ω as burden resistance. From the obtained results, neither 87L and Δ87L presented incorrect operations, so that the relay did not display a trip signal. Hence, for the external faults with CT saturation simulations assessed, graphical performance analysis with operation time are not displayed.

V. Conclusions

In order to guarantee the correct operation of the differential protection phase elements, by eliminating the influence of the pre-fault conditions, this paper dealt with the evaluation of the conventional and incremental methods, through the analysis of the phase elements trajectories. Thus, the equations that describe the trajectories on the alpha plane due to faults on transmission lines were demonstrated and later tested by means of computational and experimental analyses.

The results revealed that the healthy phases elements present a constant location on the alpha plane, at point $(-1; 0)$, which characterizes a stability point. Regarding the faulted phases,

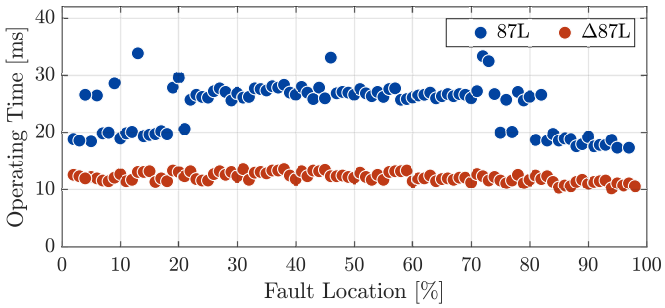

Fig. 10: AG Fault - Fault Location Variation

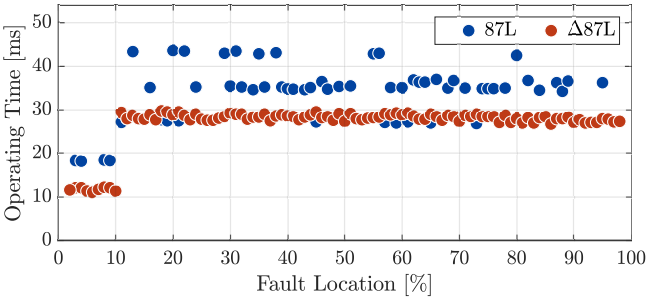

Fig. 11: BC Fault - Fault Location Variation

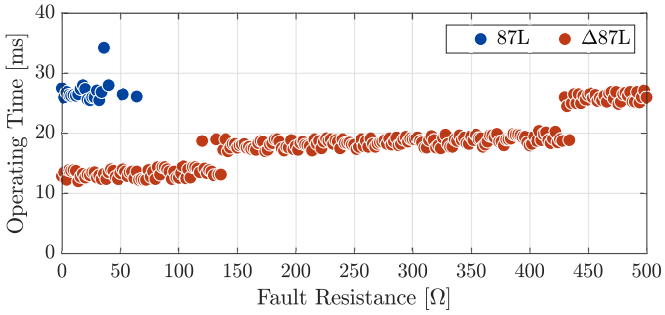

Fig. 12: AG Fault - Fault Resistance Variation

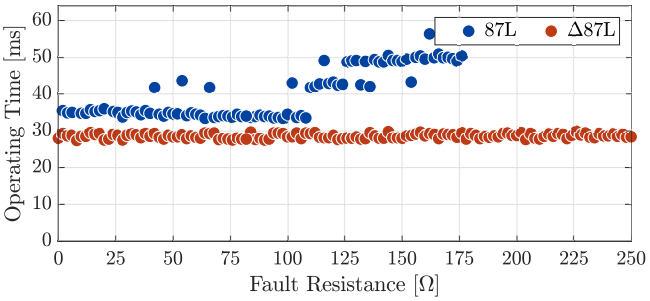

Fig. 13: BC Fault - Fault Resistance Variation

the trajectory of the CDE and IDE were explained based on the equations displayed in Table II. From these analyses, it was also observed how the fault resistance and load condition variation influenced the CDE trajectories. On the other hand, the IDE remains stable in the operation zone as they are not influenced by R_G and δ. In addition, it was observed that the fault location and the source-to-line impedance ratio affect both the CDE and IDE trajectories, considering that these parameters influence the calculation of C_j. It is noteworthy to mention that the performance of Δ87L is more consistent when compared to the 87L by means of their operating times, under multiple fault conditions.

In the presented paper the equations deductions and mappings of the conventional and incremental elements trajectories evaluations are performed considering all four types of fault. Therefore, the analyses based on all types of fault stand out as contributions of this work, once only the trajectories of the conventional and incremental differential elements for a single-phase short circuit are deduced among papers available in the literature. These analyses developed in conjunction with tests on commercial relays are sufficient to validate the deducted equations, in addition to infer exactly how different operation conditions interfere on the trajectories.

Besides the favorable performance presented in the evaluated results, it is important to note that the use of incremental differential protection does not depend on pickup and slope settings rearrangements. The Δ87L also does not require additional logic, linked to voltage measurement, to compensate the charging current of the protected line. To this extent, one can conclude that the Δ87L element can be simply implemented and easily integrated and employed to enhance the performance of the conventional differential element in real devices applications, ensuring that the protection logic will correctly operate despite pre-fault system conditions.

REFERENCES

[1] G. Ziegler, *Numerical Differential Protection: Principles and Applications*, 2nd ed. Berlin: Siemens, 2012.

[2] J. Roberts, D. Tziouvaras, G. Benmouyal, and H. Altuve, "The effect of multiprinciple line protection on dependability and security," Schweitzer Engineering Laboratories Inc., Pullman, WA, Tech. Rep., 2001.

[3] H. Altuve, G. Benmouyal, J. Roberts, and D. A. Tziouvaras, "Transmission line differential protection with an enhanced characteristic," vol. 2, pp. 414–419 Vol.2, Abril 2004.

[4] D. A. Tziouvaras, H. Altuve, G. Benmouyal, and J. Roberts, "Line differential protection with an enhanced characteristic," Schweitzer Engineering Laboratories Inc., Pullman, WA, Tech. Rep., 2003.

[5] H. J. A. Ferrer and I. Edmund O. Schweitzer, "Modern solutions for protection, control and monitorin of eletronic power system," Schweitzer Engineering Laboratories Inc., Tech. Rep., 2010.

[6] J. Roberts, D. Tziouvaras, G. Benmouyal, and H. Altuve, "The effect of multiprinciple line protection on dependability and security," in *54th Annual Conference for Protective Relay Engineers*, 2001, pp. 3–5.

[7] B. Kasztenny, G. Benmouyal, H. J. Altuve, and N. Fischer, "Tutorial on operating characteristics of microprocessor-based multiterminal line current differential relays," *Present Problems of Power System Control*, 2013.

[8] Hank Miller and John Burger and Normann Fischer and Bogdan Kasztenny, "Modern Line Current Differential Protection Solutions." Texas, USA: Texas A&M Conference for Protective Relay Engineers, 2010.

[9] Xue, Yiyan and Finney, Dale and Le, Bin, "Charging Current in Long Lines and High-Voltage Cables—Protection Application Considerations," in *67th Annual Georgia Tech Protective Relaying Conference, Atlanta, Georgia,(May 8-10, 2013)*, 2012, pp. 1–17.

[10] Xue, Yiyan and Kasztenny, Bogdan and Taylor, Douglas and Xia, Yu, "Series compensation, power swings, and inverter-based sources and their impact on line current differential protection," in *2013 66th Annual Conference for Protective Relay Engineers*. IEEE, 2013, pp. 80–91.

[11] G. Benmouyal, "The trajectories of line current differential faults in the alpha plane," Schweitzer Engineering Laboratories Inc., Pullman, WA, Tech. Rep., 2005.

[12] G. Benmouyal and J. B. Mooney, "Advanced sequence elements for line current differential protection," Schweitzer Engineering Laboratories Inc., Pullman, WA, Tech. Rep., 2006.

[13] M. L. S. Almeida and K. M. Silva, "Transmission lines differential protection based on an alternative incremental complex power alpha plane," *IET Generation, Transmission & Distribution*, vol. 11, pp. 10–17, 2017.

[14] A. R. Warrington, *Protective Relays: Their Theory and Practice, Volume 1*, 1st ed. London: Chapman & Hall, 1962.

[15] LEUVEN, EMTP CENTER, "ATP Rule Book," 1987.

[16] T. Bi, Y. Yu, S. Huang, and Q. Yang, "An accurate compensation method of distributed capacitance current in differential protection of uhv transmission line," in *Power Engineering Society General Meeting*. June, 2005.

[17] V. G. Machado *et al.*, "Lt 500 kv interligação norte sul iii - trecho 2 solução estrutural com torre estaiada monomastro e feixe expandido," in *Proc. of the XIX SNPTEE - In Portuguese*, Rio de Janeiro, Brazil, October, 2007.

[18] IEEE,, "EMTP reference models for transmission line relay testing," *URL http://www. pes-psrc. org*, 2004.

[19] Pajuelo, E and Ramakrishna, G and Sachdev, MS, "Phasor estimation technique to reduce the impact of coupling capacitor voltage transformer transients," *IET generation, transmission & distribution*, vol. 2, no. 4, pp. 588–599, 2008.